Nuclear Instruments and Methods in Physics Research A 619 (2010) 47–50

Contents lists available at ScienceDirect

Nuclear Instruments and Methods in Physics Research A

journal homepage: www.elsevier.com/locate/nima

An improvement to the full-foil mapping technique for high accuracy measurement of X-ray mass attenuation coefficients

Nicholas A. Rae, Jack L. Glover, Christopher T. Chantler *

School of Physics, University of Melbourne, Victoria 3010, Australia

ARTICLE INFO

Available online 1 February 2010

Keywords:
X-ray mass attenuation coefficient
Atomic form-factor
XERT

ABSTRACT

The limiting uncertainty in recent high accuracy measurements of the mass attenuation coefficient is the measurement of the integrated column density. An improvement in the design of the absorption foil holder is described which reduces the integrated column density uncertainty. The new design allows the edges of the foil to be more accurately mapped by the X-ray beam by reducing the largest source of uncertainty in the foil mapping: the uncertainty in the points along the foil edge. The method is shown to reduce the uncertainty in measurements of the mass attenuation coefficient of zinc foils. The reduced uncertainty in the full-foil mapping will allow the X-ray Extended Range Technique (XERT) to be applied to small non-metallic absorption foils more accurately.

1. Introduction

In high accuracy measurements made with the X-ray Extended Range Technique (XERT), the limiting factor in the uncertainty of the results has been the determination of the integrated column density. In almost all other reported measurements of absorption or attenuation, this has also been a key weak link in estimation of uncertainty. The full-foil mapping technique has been developed as part of the XERT to measure the integrated column density to high accuracy. Here we present improvements to the full-foil mapping technique which have lead to higher accuracies in the measured mass attenuation coefficients of zinc.

X-ray mass attenuation coefficients have a wide range of applications in X-ray science. Many theoretical calculations have been made and currently two such calculations are supported by the National Institute of Standards and Technology (NIST); FFAST [1] and XCOM [2]. However, significant discrepancies exist between theory and theory, theory and experiment [3], and experiment and experiment [4,5]. High accuracy measurements are needed to distinguish between the discrepant calculations [6,7].

Recent measurements off the mass attenuation coefficient across a wide range of X-ray energies have been made using the XERT for molybdenum [8], copper [9] and silver [10]. In all of these measurements, large discrepancies have been seen between the measurements and the theories of FFAST and XCOM, especially in the region between the K-edge and up to about 2.5 keV above the edge.

In these cases, the XERT has been applied to measurement for high purity metal foils. Metal foils are well suited to attenuation measurements because they can be rolled or pressed to optimal thicknesses for X-ray absorption (typically between 10 and 100 μm), while having a large cross-sectional area, in this case 25.4 mm square.

The full-foil mapping is used in the XERT to determine the mass attenuation coefficient on an absolute scale. The X-ray beam is mapped across the surface of the foil. The average integrated column density can then be calculated from the foil area and mass which can be measured to high accuracy. The larger the area mapped compared to the beam size the more accurately the mass attenuation coefficient can be determined from the average integrated column density.

Elemental or binary compound non-metallic materials are much more difficult to manufacture than metal foils for absorption experiments. They are typically much more brittle than metals and cannot be rolled or pressed. When they have a large (greater than 5 mm^2) two-dimensional cross-sectional area, it becomes difficult produce them with a thickness between 10 and 100 μm (suitable for absorption measurements) because of their brittle nature.

Some single crystals such as silicon and silicon compounds can be made suitable for high accuracy absorption measurements. The XERT has been applied to measurements of silicon [11]. However, single crystals produce large Bragg reflection peaks. These peaks affect the measured mass attenuation coefficient, limiting the accuracy of the measurements. Measurements have also been made on cadmium vapor [12,13] and compared to theoretical calculations. Difficulties in the absolute measurement of these vapour systems arise from the uncertainty in pressure and in the transfer standards.

* Corresponding author.
E-mail address: chantler@physics.unimelb.edu.au (C.T. Chantler).

0168-9002/$ - see front matter © 2010 Elsevier B.V. All rights reserved.
doi:10.1016/j.nima.2010.01.067

The determination of the mass attenuation coefficient on an absolute scale from the mass and area of the foil requires that the integrated column density of the foil is measured. Any part of the foil surface which is not measured by the beam may affect the result of the average the integrated column density if it has higher or lower attenuation then the average for the foil. We therefore ensure that every part of the foil is included in the average.

Here we describe modifications to the absorption foil holder which make it possible to measure the integrated column density at every point on the foil surface more easily. The new design has less overlap between the perspex holder and the foil. In previous studies, non-linear least squares fitting has been used to correct for the attenuation of perspex in regions of overlap between perspex and foil. This was necessary to ensure that every part of the foil is included in the average integrated column density. With the new design, there are only two small regions of overlap along the edges of the foil. The uncertainty due to fitting the perspex holder profile has been reduced by reducing the size of the overlapping regions.

By maximizing the region of the foil surface which with no perspex overlap, smaller absorption foils can used. This has allowed us to extend the XERT to smaller and non-metallic absorbing materials more accurately. High accuracy measurements of the attenuation of non-metallic materials will allow us to test structure and bonding effects in XAFS [14] and XANES [15] analysis more accurately. They will also widen the range of elements for which we test the theoretical calculations of XCOM and FFAST.

2. Integrated column density

The integrated column density $[\rho t]_{xy}$ is the density at point (x,y) of the foil along the path of the X-ray beam

$$[\rho t]_{xy} = \int \rho_{xyz}\, dz \tag{1}$$

where ρ_{xyz} is the three dimension density of the foil. The beam travels in the z direction and passes through the foil at the point (x,y) [16]. To determine the average integrated column density of the foil, $[\rho t]_{av}$, one measures the total mass and area of the foil:

$$[\rho t]_{av} = \frac{m}{A}. \tag{2}$$

The transmission probability of the foil P is a number between zero and one which is the fraction of the beam which is attenuated through the foil

$$P = \frac{I}{I_0}. \tag{3}$$

The absorption of the X-ray beam is then given by the Beer–Lambert law

$$\left[\frac{\mu}{\rho}\right][\rho t] = \ln\frac{I}{I_0} = \ln(P) \tag{4}$$

where I_0 is the unattended intensity and I and is the attenuated intensity of the beam. If the density of the foil is assumed to be homogeneous then the integrated column density can be related to thickness of the foil which the beam passes through and the density of the foil which can be determined from the foil mass and area. The integrated column density of the foil varies across the foil and should be mapped at each point on the foil surface and compared to the integrated column density of the foil where the X-ray beam is absorbed $[\rho t]_c$. The integrated column density at the central point of the foil $[\rho t]_c$ is determined from

$$[\rho t]_c = \frac{\left[\frac{\mu}{\rho}\right][\rho t]_c}{\left[\frac{\mu}{\rho}\right][\rho t]_{av}}[\rho t]_{av} = \frac{[\ln(P)]_c}{[\ln(P)]_{av}}\frac{m}{A}. \tag{5}$$

The integrated column density map also has the advantage that it is done in situ with the X-ray absorption experiment which avoids the potential issue of an offset in the mapping of integrated column density and the location of the absorption measurement. We choose the nominal centre of the foil to perform the absorption measurements. This is the position at which measurements of the mass attenuation coefficient are made at other energies.

To determine the mass attenuation coefficient on an absolute scale, the integrated column density must be measured at each point on the foil surface, including the edge regions. Failing to account for the integrated column density over a region of the foil surface could introduce a systematic error in the $[\rho t]_c$ if the region had a different average integrated column density to the rest of the foil. In the edge regions, only a fraction f of the beam passes through the foil. The measurements in this region must be weighted depending on the beam area which passed through the foil.

At the edges of the foil, the fraction of the beam which does not pass through the foil passes through either perspex on the right and left sides of the foil or air at the top or bottom. To determine the value of the fraction and correct for the absorption due the perspex or air-path, a 2D profile of the foil is determined and used to model the beam-fraction and foil attenuation along the foil edges.

3. Experimental details

Fig. 1 shows a schematic diagram of the experimental setup. Four zinc foils were mounted on the specimen stage. Translation stages allowed the foils to be moved vertically and horizontally about the beam. They were also necessary to map the X-ray beam across the foil in horizontal and vertical steps.

Ion chambers monitored the X-ray beam count rate upstream of the absorption foil R_0 and downstream R. The ion chambers were flowed with N_2 gas. The foil was removed from the beam to determine the X-ray absorption from other sources between the ion chambers and correct for it. The ion chamber dark currents D_0 upstream and D downstream were measured by recording the beam intensity when no beam was present. The transmission probability of the X-ray beam through the absorption foil was determined by

$$P = \left(\frac{R-D}{R_0-D_0}\right) \Big/ \left(\frac{R^B-D^B}{R_0^B-D_0^B}\right) \tag{6}$$

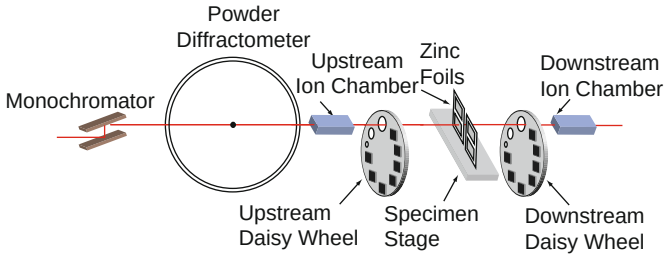

Fig. 1

where the superscript B denotes measurements made with the same removed from the beam.

The absorption foils were chosen to be high purity 99.999% zinc. The foils were weighed on a Mettler microgram balance to determine their mass m with an error of $\Delta m/m$ of 0.002%. The perimeter of the foils were mapped at 172 points using an optical comparator to determine their area A with an error $\Delta A/A$ of 0.026%.

The X-ray beam was defined by slits to be 2 mm horizontal by 0.5 mm vertical. The beam energy was chosen to be 15.2 keV using a Si (1 1 1) double bounce monochromator. Two translation stages were used to translate the foil vertical and horizontally relative to the beam. The foil was mapped in steps 2 mm horizontal by 0.5 mm vertical corresponding to the beam size.

There are four different regions of the X-ray map. At the edges of the foil, only a fraction of the beam, f, passes though the foil while the remaining fraction, $(1-f)$, passed though either the Perspex holder or air. In the central region of the foil, the beam passed through only foil and therefore f is equal to one. Because only a fraction of the beam passes through foil in the edge regions, the measurements in this region need to be corrected for the attenuation of the non-foil material.

4. Edge regions

Methods of foil edge fitting are described in this section. The first method applies to foils which have a predictable surface variation and are well described by a global model of the foil surface. An alternative method is described for foils which do not have a predictable surface variation but are better described by a model of the local surface variation.

The first method for recovering the attenuation of the edge regions of the foil is the global method. This approach is particularly suited to cases where the foil has a predictable spatial attenuation variation (e.g. a wedge-like foil or a foil with oscillations from rolling) [9].

The foil is modelled as a square or rectangle with at least three parameters describing the position and orientation of the foil. The information about orientation comes from those measurements where the X-ray beam is incident upon the edge of the foil. The spatial variation of the attenuation of the foil must also be modelled. The function describing the attenuation of the foil at point $\vec{x}$ will be denoted $F(\vec{x};\vec{P})$, where $\vec{P}$ is an array of model parameters For example, in the case of a wedge-like foil, we have

$$F(\vec{x};[\mu t]_0, m_x, m_y, x_0, y_0) = [\mu t]_0 + m_x(x-x_0) + m_y(y-y_0) \tag{7}$$

where $[\mu t]_0$ is the value of the attenuation at the centre of the foil (x_0, y_0). The sum over i is for measurements and sum over j is for the model points. The parameters m_x and m_y describe the gradients of the wedge in the x and y directions, respectively. The values and uncertainties of these parameters can be determined by fitting the model to the data taken during the full-foil mapping.

The purpose of the full-foil mapping is to accurately determine the average attenuation $[\mu t]_{ave}$. Our model $F(\vec{x};\vec{P})$ is used to estimate the attenuation at the edge regions or anywhere else we do not have measurements. The formula for the average attenuation becomes

$$[\mu t]_{ave} = \frac{1}{A}\left(\sum_i a_i[\mu t]_i + \sum_j a_j F(\vec{x}_j;\vec{P})\right) \tag{8}$$

where a_j is the area of a region centred at $\vec{x}_j$ where no suitable attenuation measurement is available.

The average attenuation is now affected by two types of uncertainties: uncertainty in the experimental measurements and the uncertainty and covariance of the model parameters. The formula for the uncertainty in the average attenuation becomes

$$\sigma^2_{[\mu t]_{ave}} = \sum_i \sigma^2_{[\mu t]_i}\left(\frac{a_i}{A}\right)^2 + \sum_{jk} COV(j,k)\left(\frac{\partial^2[\mu t]_{ave}}{\partial P_j \partial P_k}\right)^2 \tag{9}$$

where P_j is the j th element of the array of model parameters $\vec{P}$. $COV(j,k)$ is the covariance between the P_j and P_k. $\partial^2[\mu t]_{ave}/\partial P_j \partial P_k$ is the 2nd-order, mixed partial-derivative of the average attenuation of the foil with respect to P_j and P_k. The first summation gives the uncertainty contribution from the experimental measurements and the second summation gives the contribution from the uncertainty and covariance of the model parameters.

This method performs well for foils that show predicable spatial variation of attenuation. It correctly accounts for the uncertainty and correlation in the model parameters associated with recovering the attenuation of the edge points.

This method recovers the attenuation of the edge regions of the foil by global extrapolation of the full-foil map.

When the surface variation of the foil is not well described by a global model, an alternative approach is to model the surface variation locally to the edge points for which the attenuation is to be recovered. An example is the model of the foil attenuation in the direction perpendicular to the edge points with a polynomial. The distance away from the edge that the model is applied, and the order of the polynomial used to fit are varied until a model which has the smallest χ^2_{red} is obtained. The uncertainty and covariance of the model parameters contributes to the uncertainty in the attenuation as described in Eq. (9). This method was used for the zinc foils.

To quantify the improvement in accuracy due to the inclusion of the foil edge regions, the mass attenuation coefficient of the foil and percentage error were calculated with the edge and adjacent regions excluded. The accuracy of the mass attenuation coefficient of 0.148% without edge correction was improved to 0.045% when the edges are correctly taken into account. For high accuracy measurements, the edge correction significantly reduces the total uncertainty, accounting for about one fifth of the error in this case. Fig. 2 shows that the uncertainty in measurements made near the foil edges is much higher than in the central region. It is also important to note that any edge regions of the foil not measured directly with the X-ray beam may have a systematically different integrated column density from that of the rest of the foil. An example is at the thin or thick ends of a edge wedge shaped foil. To avoid such systematic variations skewing calculations of the mass attenuation coefficient, any regions not directly mapped by the X-ray beam must be assigned an appropriately larger uncertainty.

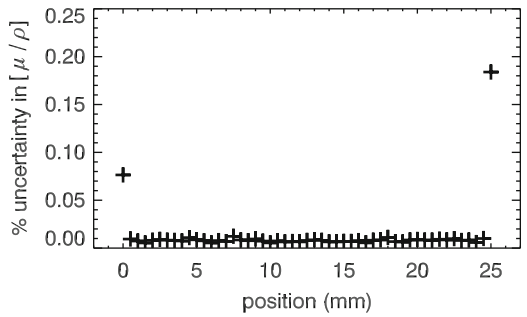

Fig. 2. The percentage uncertainty in the mass attenuation coefficient along a cross-section of the foil surface. In the central region the uncertainty is much lower than at the left and right edges of the foil. The new holder design maximizes the central region of the foil, minimizing the foil regions with large uncertainties.

5. Conclusion

The new foil holder design minimizes the region in the full-foil area scan where the beam passes through both the perspex holder and the absorption foil. This reduced the uncertainty from the non-linear least squares fitting of the perspex holder profile. Smaller foils may be now be used to obtain high accuracy measurements. This allows us the extend XERT to non-metallic materials with different structure and bonding to test XAFS and XANES calculations. Taking account of the edge regions leads to more accurate mass attenuation measurements for zinc foils.

It is important that the whole foil surface is accounted for when determining the average integrated column density. Absorption foils may have variations in thickness and density which would affect the measured mass attenuation coefficient if some regions of the sample not included in the full-foil map. The edge regions, where only a fraction of the beam passes through the foil, require fitting to obtain the correct integrated column density. A significant improvement was made to the accuracy of the mass attenuation coefficient from 0.148% to 0.045% without the edge correction.

Acknowledgements

The authors acknowledge the experimental team and the local ANBF staff, particularly James Hester, as well as funding from the Australian Synchrotron Research Program and Australian Research Council.

References

[1] C.T. Chantler, J. Phys. Chem. Ref. Data 29 (2000) 597.
[2] M.J. Berger, J.H. Hubbell, S.M. Seltzer, J. Chang, J.S. Coursey, R. Sukumar, D.S. Zucker, NIST Standard Ref. Database 8 (1998) 87.
[3] A. Karabulut, A. Gurol, G. Budak, R. Polat, Eur. Phys. J. D Atoms Molecules Clusters Opt. Phys. 21 (2002) 57.
[4] D.C. Creagh, J.H. Hubbell, Acta Crystallogr. 43 (1987) 102.
[5] D.C. Creagh, J.H. Hubbell, Acta Crystallogr. 46 (1990) 402.
[6] L. Gerward, G. Thuesen, S. Jensen, I. Alstrup, Acta Crystallogr. Sect. A 35 (1979) 852.
[7] L. Gerward, Acta Crystallogr. Sect. A Found. Crystallogr. 45 (1989) 1.
[8] M.D. de Jonge, C.Q. Tran, C.T. Chantler, Z. Barnea, B.B. Dhal, D.J. Cookson, W.-K. Lee, A. Mashayekhi, Phys. Rev. A 71 (2005) 032702/1.
[9] J.L. Glover, C.T. Chantler, Z. Barnea, N.A. Rae, C.Q. Tran, D.C. Creagh, D. Paterson, B.B. Dhal, Phys. Rev. A 78 (2008) 52902.
[10] C.Q. Tran, C.T. Chantler, Z. Barnea, M.D. de Jonge, B.B. Dhal, C. Chung, D. Paterson, P. Lee, J. Wang, D.J. Cookson, J. Phys. B 38 (2005) 89.
[11] C.Q. Tran, C.T. Chantler, Z. Barnea, D. Paterson, D.J. Cookson, Phys. Rev. A 67 (2003) 042716/1.
[12] A. Kodre, J. Padežnik Gomilšek, A. Mihelič, I. Arčon, Rad. Phys. Chem. 75 (2006) 188.
[13] A. Mihelič, A. Kodre, I. Arčon, J.P. Gomilšek, Acta Chim. Slov. 51 (2004) 33.
[14] J.J. Rehr, R.C. Albers, S.I. Zabinsky, Phys. Rev. Lett. 69 (1992) 3397.
[15] Y. Joly, J. Phys. B 63 (2001) 125120.
[16] M.D. de Jonge, Z. Barnea, C.T. Chantler, C.Q. Tran, Meas. Sci. Technol. 15 (2004) 1811.